(Submitted to *Int. J. Robotics Research*)
(Revised Version of IJ 1023)

Transparent Bilateral Teleoperation under Position and Rate Control

Septimiu E. Salcudean Ming Zhu Wen-Hong Zhu Keyvan Hashtrudi-Zaad

Department of Electrical & Computer Engineering
University of British Columbia
2356 Main Mall, Vancouver, B.C., Canada V6T 1Z4

Abstract

A four-channel control architecture has been suggested in the literature to achieve "transparency" for master-slave teleoperator systems under position control. In this article, the result is generalized to include teleoperator systems that are under rate control or more general master-slave kinematic correspondence laws, such as a mixed position/rate mode. A one degree-of-freedom example is given to outline the design and analysis of such a system for transparency and stability. The validity of the theory has been verified through simulations and experiments.

1 Introduction

¿From its early use in the remote manipulation of radioactive materials, the meaning of teleoperation has expanded to include manipulation at a different scale and in virtual worlds (Kazerooni 1989; Yan and Salcudean 1996; Parker et al. 1993; Hunter et al. 1989; Salcudean et al. 1997; Iwata 1990; and DiMaio et al. 1998). Teleoperation systems have the potential to play an important role in future remote or hazardous operations such as space and undersea exploration and servicing, forestry and mining, as well as in delicate operations such as microsurgery and microassembly.

Most of the early teleoperation system designs had kinematically similar master and slave because of the simplicity of the required controller. Corresponding joint servos between the master and the slave were tied together through electrical means. As a result, only position control in which the

position of the master is interpreted as a position command to the slave could be used. Later, multi-degree-of-freedom joysticks were used as input devices to command the slave manipulators (Bejczy and Handlykken 1981). Joysticks can be used universally, take little space by comparison to kinematically equivalent masters, and are less tiresome to use. Rate control, in which the position of the master is interpreted as a velocity command to the slave, can be used to position the slave in resolved-motion mode. Conventional resolved-motion position control can also be implemented over a limited motion range. For example, the space shuttle remote manipulator system is provided with both position and rate control modes.

Contact information is helpful to the operator in reducing contact forces, and therefore reducing damage to the manipulated object. It also helps an operator in probing an uncertain environment, and reduces task completion time (Stokic et al. 1986). Although this information can be provided by a visual display, the haptic channel is faster and more natural when multiaxial operation is involved. When the contact force is reflected via the master actuator to the operator's hand, the teleoperator system is said to be bilateral or force-reflecting.

Besides stability which is the fundamental requirement for any control system, bilateral controllers are designed to provide operators with teleoperation systems that are as *transparent* as possible (for a limited survey refer to (Salcudean 1998)). By transparent, it is meant that the master should feel to the operator as if the task were being manipulated directly. Appropriate meanings for *transparency* have been pursued by Yokokohji et al. (1994). In general, the requirement has been that the position/force responses of the teleoperator master and slave be identical. Clearly, this definition only applies to those teleoperator systems in which the slaves are controlled to follow the motion of the masters faithfully. In many applications, the position mapping between the master and slave needs to be scaled either down or up, or rate control needs to be used, especially if the master has a limited workspace. For such situations, transparency is better quantified in terms of the match between the mechanical impedance of the environment encountered by the slave and the mechanical impedance transmitted to or *felt* by the operator at the master (Hannaford 1990; Lawrence 1993).

Lawrence (1993) has analyzed the performance of position-controlled bilateral teleoperators,

and has indicated that none of the conventional two-channel control architectures(position-position, position-force, etc.) lead to perfect transparency, defined as an exact match between the environment impedance and the impedance transmitted to the operator for any environment impedance. Instead, a four-channel architecture using the sensed master and slave forces and positions is required. Whether a designer uses such a four-channel architecture or another approach, tradeoffs between performance and stability robustness are always necessary. Therefore, it is important to characterize the full range of achievable performance. Performance limitations of the position-force teleoperation controller have been studied by Daniel and McAree (1998), who identify the slave-master mass ratio as the key performance-determining factor. Based on a single DOF linear model and using the root-locus approach, they derive an expression for the maximum force reflection ratio that guarantees stability against pure-stiffness environments and investigate the effects on stability of various compensation schemes, such as changing the master stiffness and damping. Trade-offs between transparency and stability robustness for four-channel architectures have been presented in (Lawrence 1993; Yan and Salcudean 1996; and Hashtrudi-Zaad and Salcudean 1999).

In this article, the formalism developed in (Lawrence 1993) is used to show that, under ideal conditions, perfect transparency can be achieved by four-channel teleoperator systems that are not necessarily controlled in position mode. In particular, systems that operate in rate control mode, in which the slave velocity tracks the master position, a combination of rate and position mode, or a general frequency weighted master-slave kinematic correspondence law, can still transmit an impedance to the master that perfectly matches the environment impedance encountered by the slave, regardless of the environment impedance.

Without loss of generality, the article considers only the one-dimensional case. The network equivalent representation of teleoperators in Section 2 is followed by a review of the Lawrence formalism in Section 3. Section 4 describes the design and analysis of a transparent four-channel architecture for position control mode, and Section 5 gives conditions for transparency in rate mode or other kinematic correspondence modes. Sections 6 and 7 present simulation and experimental results that support the

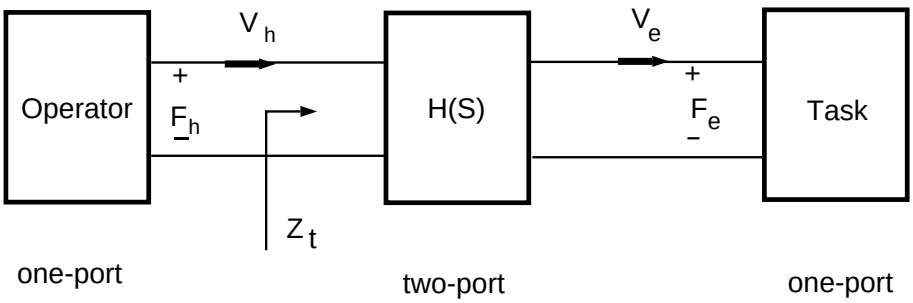

Figure 1: Network representation of teleoperator system.

theoretical work and conclusions are drawn in Section 8.

2 Network Representation of Teleoperator Systems

Figure 1 shows a network model of a telemanipulation system consisting of a master-slave two-port network terminated by two one-ports, the operator and the environment (Anderson and Spong 1989; Hannaford 1989). An n-port network is characterized by the relationship between effort, f (force, voltage) and flow, v (velocity, current). Assuming linear time-invariant (LTI) lumped dynamical models for the operator's hand and the environment and no exogenous force/velocity sources, the relationship between v_e and f_e, and v_h and f_h are specified by the operator and the environment impedances Z_e and Z_h, respectively, according to

$$Z_e(s) := \frac{F_e(s)}{V_e(s)} \quad , \quad Z_h(s) := \frac{F_h(s)}{-V_h(s)} \ , \tag{1}$$

where V_h, V_e, F_h, and F_e represent the Laplace transforms of the the hand velocity, the environment velocity, the hand force on the master, and the slave force on the environment, respectively . An LTI lumped master-slave two-port network can be represented by its hybrid matrix $\underline{H}(s) = [\underline{h}_{ij}], i, j = 1, 2$, defined as

$$\begin{bmatrix} F_h \\ -V_e \end{bmatrix} = \begin{bmatrix} \underline{h}_{11} & \underline{h}_{12} \\ \underline{h}_{21} & \underline{h}_{22} \end{bmatrix} \begin{bmatrix} V_h \\ F_e \end{bmatrix} \ , \tag{2}$$

where it is assumed that the operator and the environment are in contact with the master and slave, respectively. Using the master-slave network hybrid parameters (2) and the task impedance in (1), the

transmitted impedance Z_t felt by the operator can be expressed as

$$Z_t := \frac{F_h}{V_h} = \frac{\underline{h}_{11}(1 + \underline{h}_{22}Z_e) - \underline{h}_{21}\underline{h}_{12}Z_e}{1 + \underline{h}_{22}Z_e} \quad . \tag{3}$$

Thus, the following necessary and sufficient condition set for transparency must hold (Hannaford 1989):

$$\underline{h}_{11} = \underline{h}_{22} = 0 \tag{4}$$

$$\underline{h}_{12}\ \underline{h}_{21} = -1 \tag{5}$$

3 General Teleoperator Structure

In a conventional position controlled teleoperator system, either the environment contact force or the slave position is fed back to the master to provide force reflection. The former is called *direct force feedback* method, and the latter *coordinating force feedback* method. ¿From the network point of view, there are no specific reasons for not using the position and force information bilaterally. Such a four-channel communication scheme gives more freedom to achieve the hybrid matrix desired for transparency. Figure 2 shows a block diagram of a general teleoperator structure, where the formalism presented in the earlier work by Lawrence (1993) is adopted. In particular, an example by Salcudean and Wong (1993) shows the symbol blocks as:

$$Z_m \ := \ M_m s \quad , \quad C_m := B_m + \frac{K_m}{s} \tag{6}$$

$$Z_s \ := \ M_s s \quad , \quad C_s := B_s + \frac{K_s}{s} \ , \tag{7}$$

where the master and slave manipulator dynamics are approximated by simple masses M_m and M_s, C_m and C_s denote local master and slave proportional plus derivative controller transfer functions, $C_1, \cdots, C_4$ are the remote feedback controller transfer functions, and F_h^* and F_e^* are the hand and environment exogenous input forces, respectively. It is easily seen that the position-position and position-force architectures are two special cases of this general control structure by setting $C_2 = C_3 = 0$ and $C_3 = C_4 = 0$, respectively.

The transmitted impedance felt by the operator can be derived in terms of the block transfer

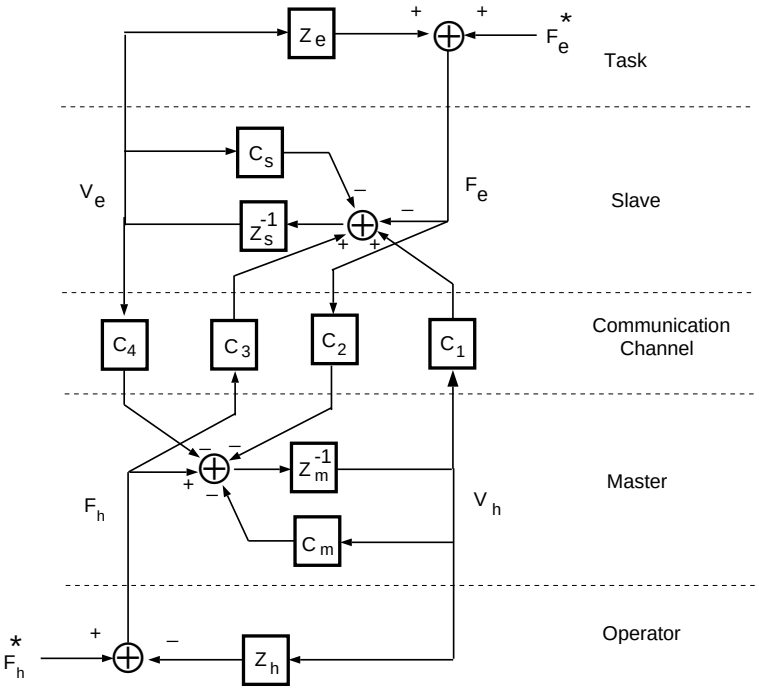

Figure 2: General teleoperator structure: after Lawrence (1993).

functions as

$$Z_t = \frac{[(Z_m + C_m)(Z_s + C_s) + C_1C_4] + (Z_m + C_m + C_1C_2)Z_e}{(Z_s + C_s - C_3C_4) + (1 - C_2C_3)Z_e} \tag{8}$$

with the difference between Z_t and Z_e being interpreted as a measure of transparency (Lawrence 1993). Stability of the closed-loop system can be checked by applying the Nyquist criterion to the loop gains $LG1$ and $LG2$ in Figure 3, created by reorganizing the block diagram of the general teleoperator system of Figure 2. In the sequel, for stability analysis purposes, it is assumed that the operator and task impedances are passive (Hogan 1989).

4 Transparency Under Position Control

For position mode control, it can seen from (8) that a perfectly transparent teleoperation system, *i.e.*, one that satisfies

$$Z_t = Z_e \quad \text{for any } Z_e \ , \tag{9}$$

can be achieved if and only if the condition-set

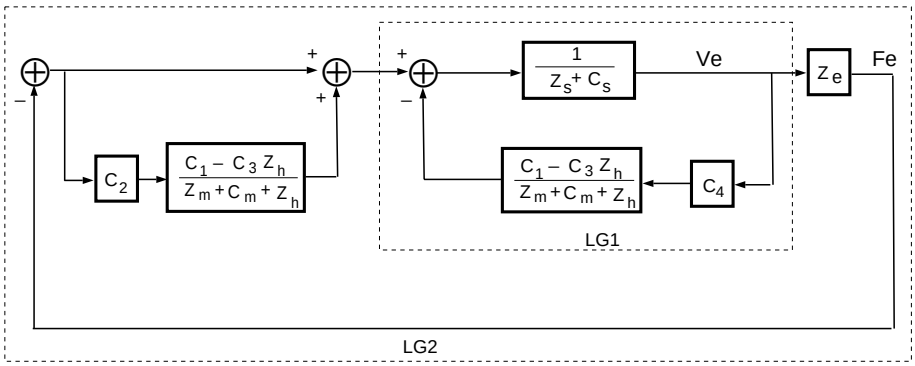

Figure 3: Closed-loop stability analysis.

$$\begin{cases} C_1 &= Z_s + C_s \\ C_2 &= 1 \\ C_3 &= 1 \\ C_4 &= -(Z_m + C_m) \end{cases} \tag{10}$$

is satisfied. It is interesting to note that the end point impedance of the system viewed from the slave side equals

$$Z_{end} = -\frac{F_e}{V_e} = -\frac{F_h}{V_h} = Z_h \tag{11}$$

which is the impedance of the human hand. In robot control, the goal of impedance control of a manipulator is to create a desired impedance at its end-effector. However, in practice, it is not very clear what impedance is the best for manipulators in contact tasks. Experience shows that human hands offer adjustable impedances (Fasse and Hogan 1994), which makes them ideal for manipulating almost any object without encountering stability problems. Thus, from the impedance control point of view, the above fully transparent teleoperator structure provides a way to reconstruct the human impedance at the manipulator end-effector.

Applying (10) to Figure 2 yields

$$F_h - F_e = (Z_m + C_m)(V_h - V_e) \tag{12}$$

$$F_h - F_e = (Z_s + C_s)(V_e - V_h) \tag{13}$$

and consequently, the position error dynamics can be formed as

$$s(Z_m + C_m + Z_s + C_s)(X_h - X_e) = 0 \tag{14}$$

where X_h and X_e are the positions of the master and slave, respectively. With Z_m, Z_s, C_m, and C_s as defined in (6)-(7), the teleoperation system is stable and the slave tracks the master position asymptotically.

However, the ideal controller described in (10) cannot be implemented exactly, as perfect knowledge of the master and slave masses and perfect sensing and actuation (with infinite dynamic range), including acceleration sensing, would be required in order to implement C_1 and C_4. As well, perfect transparency might not be desirable. Indeed, the master and slave would drift around if neither were connected to the operator and/or the environment. One can therefore modify the original design (10) by ignoring the master and slave mass dynamics at the expense of a departure from the transparency model at higher frequencies, as follows:

$$\begin{cases} C_1 &= C_s \\ C_2 &= 1 \\ C_3 &= 1 \\ C_4 &= -C_m \end{cases} \tag{15}$$

With this controller, (12)–(13) become

$$F_h - F_e = Z_m V_h + C_m(V_h - V_e) \tag{16}$$

$$F_h - F_e = Z_s V_e + C_s(V_e - V_h) \ . \tag{17}$$

When the master and slave are identical, that is $Z_m = Z_s$, the position error dynamics is simplified to

$$s(Z_m + C_m + C_s)(X_h - X_e) = 0 \ , \tag{18}$$

indicating that the slave and master positions track each other asymptotically. In addition, substituting (15) into (8) yields

$$Z_t = Z_m + Z_e \ , \tag{19}$$

meaning that the operator indeed feels the environment impedance Z_e added to an "intervenient" or "tool" impedance Z_m. While in this particular example Z_m is just a mass, as suggested by Salcudean et al. (1995), local control of the master can be used to modify this impedance by adding damping and a centering stiffness. These are desirable in order to improve fine motor control and prevent the master and slave from drifting. As a result, a small force is always needed to move the telemanipulator even

without a payload. The concept of *intervenient impedance* was proposed by Yokokohji and Yoshikawa (1994) to guarantee system stability robustness to communication-channel time-delay. The impedance transmitted by the slave to the environment equals

$$Z_{end} = Z_m + Z_h \tag{20}$$

which is the impedance of the human hand plus an intervenient impedance.

In general, system stability can be checked by applying the Nyquist criterion to LG1 and LG2 in Figure 3. However, for this simple model, the inner loop can be simplified by incorporating the control law (15) and its closed-loop stability can be determined by checking the location of the characteristic equation zeros. When $Z_m = Z_s$, the inner loop is stable as the characteristic equation

$$LG1_{open} + 1 = \frac{(Z_s + C_s + C_m)(Z_h + Z_m)}{(Z_m + C_m + Z_h)(Z_s + C_s)} = 0 \tag{21}$$

has no right-half-plane zeros, since Z_h is passive. Consequently, the characteristic equation of the outer loop becomes

$$LG2_{open} + 1 = \frac{(Z_h + Z_m + Z_e)(Z_m + C_m + C_s)}{(Z_m + Z_h)(Z_s + C_s + C_m)} = 0 \tag{22}$$

which also has no zeros in the right-half plane, since Z_h and Z_e are passive. The above simplified stability analysis is based on the assumption that the master and slave dynamics are identical. It is not always possible to make $Z_m = Z_s$, as local frequency-dependent compensation must be applied. However, in some cases, motion and force scaling can be used to achieve $Z_m = Z_s$. For example, if $Z_s/Z_m = \delta > 1$, then $Z_m = Z_s$ can be achieved by scaling the V_e units up by δ_1, $V_e = \delta_1 \underline{V}_e$, and the F_e units down by δ_2, $F_e = (1/\delta_2)\underline{F}_e$, subject to $\delta = delta_1\delta_2$, where $\underline{V}_e$ and $\underline{F}_e$ are the slave velocity and force before scaling.

The above analysis is based on the assumptions that the force measurements are accurate and the communication delay between the master and slave system is negligible. Depending on values of the hand and environment impedances, Salcudean and Wong (1993) report that errors of only 5% in the force feedforward terms can drive the system into instability. As well, significant delays have been shown to degrade stability robustness (Yokokohji and Yoshikawa 1994; Lawrence 1993;

Hashtrudi-Zaad and Salcudean 1999; and Daniel and McAree 1998). The extent to which stability robustness is compromised in order to achieve transparency can be higher in transparency-optimized four-channel control architectures than it is in conventional two-channel architectures (Hashtrudi-Zaad and Salcudean 1999). The robust implementation of the above scheme requires further investigation.

Note that the dynamics cancellation does not work well in many situations. However, by using careful dynamic modeling and computed-torque style controllers, on carefully designed hardware, one can significantly alter the mechanical impedance of a device without loosing stability. For example, in work by (Sirouspour et al. 2000), changes of the mass of a haptic device from 50% to 1000% of the nominal have been possible without losing stability. Perfectly transparent controllers define a goal from which the designer can intelligently back away from by using passivity tools such as Llewellyn's absolute stability criterion (Adams and Hannaford 1999) or its multi-input-multi-output structured singular value counterpart. In the process, a certain level of intuition is preserved that would be lost if the controller design problem would be cast from the beginning into a large frequency shaping problem as done, for example, in (Yan and Salcudean 1996). Successful designs following this approach have been presented for haptic devices (Adams and Hannaford 1999; Sirouspour et. al. 2000).

5 Transparency Under General Master-Slave Kinematic Correspondence

The position/force architecture does not provide transparency, nor does the rate/force one. As discussed before, for position mode control, the bilateral communication of force information is important in achieving transparency. In this section, we extend the previous result to include a more general kinematic correspondence between identical master and slave manipulators.

As before, assuming $Z_m = Z_s$, the control laws are designed as

$$\begin{cases} C_1 &= C_s/G \\ C_2 &= G \\ C_3 &= 1/G \\ C_4 &= -C_m G \end{cases} \tag{23}$$

where G is a transfer function. From Figure 3 and equation (8) it follows that (19), (21), and (22) are

still valid. Moreover, from Figure 2 and (23), the hybrid matrix of the master-slave system defined in (2) can be computed as

$$\underline{H} = \begin{bmatrix} Z_m & G \\ -1/G & 0 \end{bmatrix} . \tag{24}$$

The system is transparent modulo the intervenient impedance Z_m, as $\underline{h}_{12}$ and $\underline{h}_{21}$ are still inverses of each other. Following this, a new hybrid matrix $H = [h_{ij}], i, j = 1, 2$ is now defined as

$$\begin{bmatrix} F_h \\ G \cdot V_e \end{bmatrix} = \begin{bmatrix} h_{11} & h_{12} \\ h_{21} & h_{22} \end{bmatrix} \begin{bmatrix} V_h \\ G \cdot F_e \end{bmatrix} = \begin{bmatrix} Z_m & 1 \\ 1 & 0 \end{bmatrix} \begin{bmatrix} V_h \\ G \cdot F_e \end{bmatrix} \tag{25}$$

Consequently, the transfer function between the master and slave velocities is

$$\frac{V_e}{V_h} = \frac{1}{G} . \tag{26}$$

The transfer function G defines the kinematic correspondence between the master and the slave. It is clear that the previously addressed transparent position control structure in Section 4 is just a special case of (23) where the transfer function G is set to unity. Position scaling can be achieved easily by setting $G = K_v$, where K_v is the scaling factor. Other types of kinematic correspondence between the master and slave can be realized as long as G is stable and has a stable inverse. For example, a perfectly transparent rate control teleoperator system requires that

$$\frac{V_e}{V_h} = \frac{1}{K_v s} \tag{27}$$

which leads to an improper transfer function implementation of

$$C_2 = G = K_v s . \tag{28}$$

In order to prevent the controller from using force derivative signals, a first order filter can be used to achieve rate control with reasonable accuracy, that is

$$G = \frac{K_v s}{1 + Ts} \tag{29}$$

where T is a small time-constant which sets a useful low-frequency range. The system then behaves as a rate-controlled system with perfect transparency, assuming that transparency is defined by impedance matching with intervenient or tool impedance equal to that of the master.

Note that the motion/force scaling G is different from the physical scaling that might be needed to achieve $Z_s = Z_m$, as presented in the previous section. Whereas the scaling G is included in the teleoperation control framework, it is assumed that local controllers have achieved $Z_s = Z_m$ independently.

In a special case of rate control with $Z_m = 0$ and $T = 0$, where the master position is proportional to the slave velocity, impedance reflection specified by $Z_t = Z_e$ for all Z_e implies that the force felt by the operator is the derivative of the contact force. It follows that $F_h = K_v \dot{F}_e = K_v Z_e \dot{V}_e$ and $V_h = K_v \dot{V}_e$. In this case, the slave motion is the integral of the master, and the master motion is the derivative of the slave motion for all motions. Therefore, although the environment impedance is transferred without distortion to the operator, the physical correspondence between the master and the slave is changed, and features some undesirbale characteristics, such as a sticking behaviour for unilateral constraints (Parker et al, 1993). Indeed, suppose that the operator has commanded the slave to press against a rigid wall. Because a bounded F_h leads to a bounded $\dot{F}_e$, F_e cannot change instantaneously, and when the operator wishes to move the slave away from the wall by pulling back the master, the slave will "stick" to the wall. This implies that a unilateral constraint at the slave would no longer be unilateral at the master.

6 Simulation Results

In this section, a teleoperation system in which the master and slave are identical masses is considered. In order to illustrate its bahaviour in rate control and to confirm the findings of the previous section, continuous domain dynamic simulations obtained using Simulink^{TM} are presented. SI units are used throughout this paper.

The operator's hand is assumed to be a constant mass, spring and damper system with impedance model (Kazerooni et al. 1993):

$$Z_h = 0.5s + 70 + 2000/s \tag{30}$$

Each of the master and slave are assumed to have the dynamic model of the University of British

Columbia (UBC) magnetically levitated (Maglev) wrists (Salcudean et al, 1995), which can be modelled by simple masses

$$Z_m = Z_s = 0.62s \ . \tag{31}$$

Local controllers C_m and C_s were chosen as

$$C_m = C_s = 10 + 0.1/s \ . \tag{32}$$

The first set of simulations were conducted to test the free-motion behavior of the position control system with

$$G = 1 \tag{33}$$

and the rate control system with

$$G = \frac{s}{1 + 0.02s} \ . \tag{34}$$

The operator's hand force F_h^* is a square wave for both the position and rate mode simulations.

Figure 4 depicts the free-motion response. Figure 5 illustrates the same variables for a second set of simulations, with the slave in contact with a soft environment with impedance

$$Z_e = 10s + 100 + 200/s \ . \tag{35}$$

A third set of simulations are conducted to show the hard contact performance of the system controlled in position and rate modes. As shown in Figure 6, the slave is in free-motion for the first second, then it makes contact with a stiff environment with impedance

$$Z_e = 1000s + 10000 + 200000/s \ . \tag{36}$$

The slave remains in contact for the rest of the simulation. These results demonstrate the excellent position (for position control) and velocity/position (for rate control) tracking of the proposed teleoperation controller under ideal conditions.

7 Experimental Results

In this section, simulations and experiments are conducted with a 1-DOF teleoperation system.

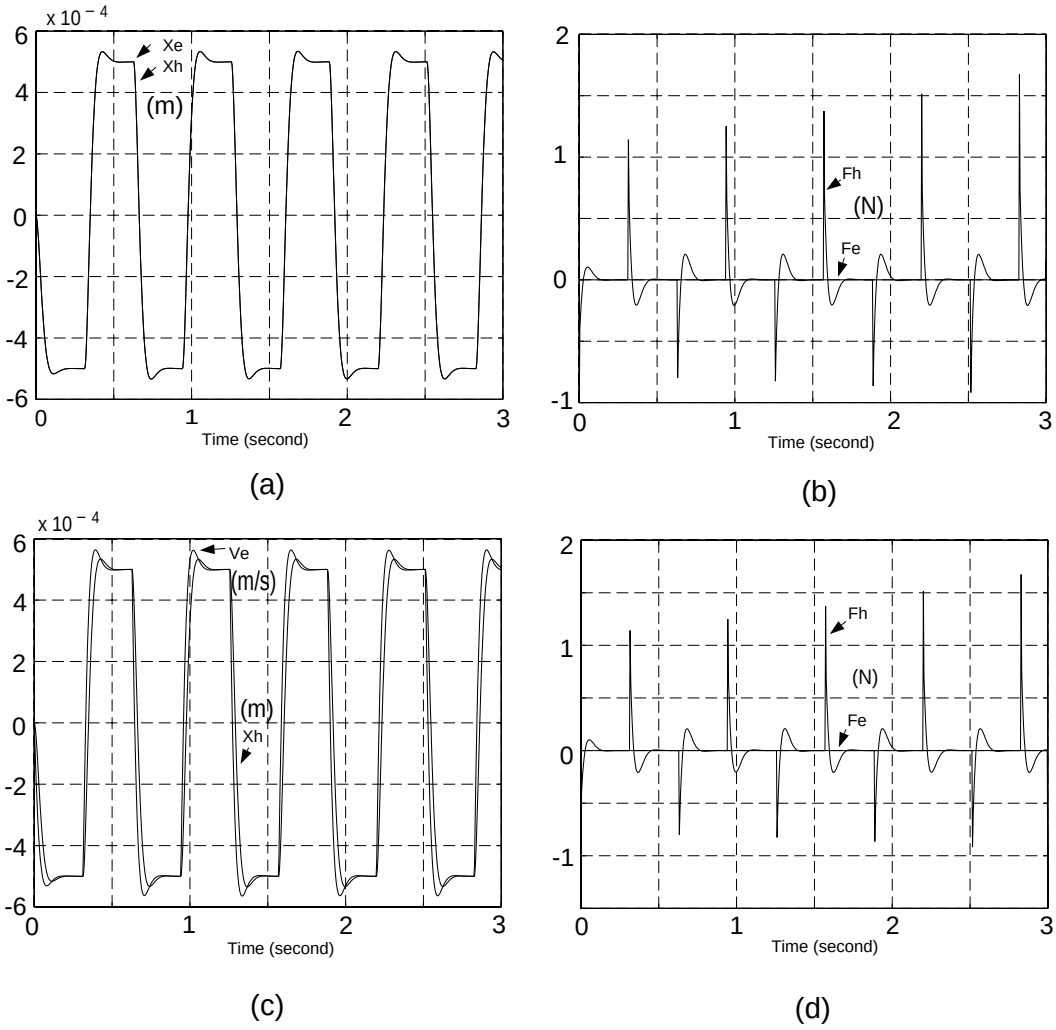

Figure 4: Transparent teleoperation: slave in free-motion. (a) and (b): position control; (c) and (d): rate control

These demonstrate that the proposed transparent rate control approach works well in a practical environment.

7.1 Experimental Set-up

As illustrated in Figure 7, the system set-up consists of a one-axis master and a one-axis slave actuated by two MAXON Motors equipped with $4,000$ pulse encoders. The master and slave motors have a planetary gearhead ($10:1$ gear-ratio) and a harmonic drive ($50:1$ gear-ratio), respectively, in order to increase output torque. Two aluminum bar linkages are mounted on the motor shaft and act as end-effector and operator handle. JR^3 wrist force sensors are used to measure the operator and environment

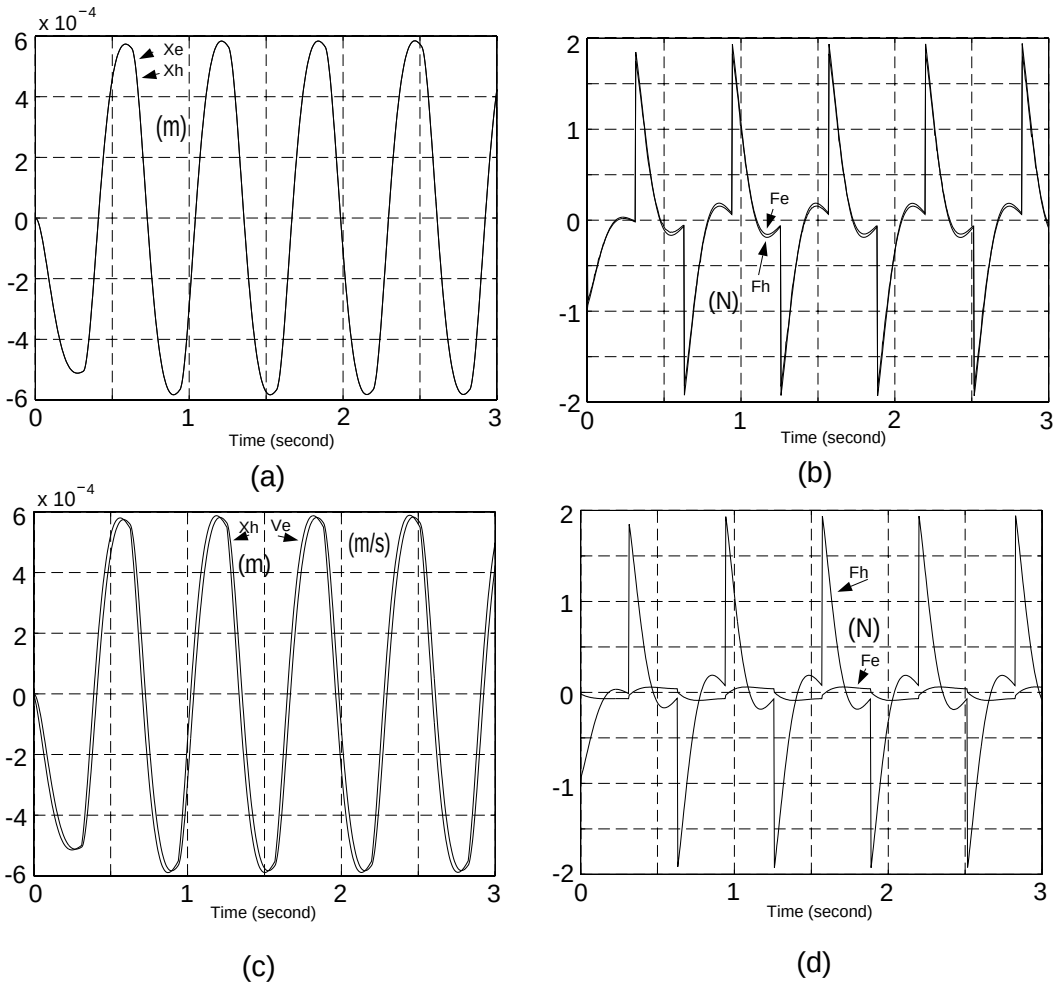

Figure 5: Transparent teleoperation: slave in contact with very soft environment. (a) and (b): position control; (c) and (d): rate control.

forces. The distances between the centers of the force sensors and the motor driving axes are 65 mm for the master and 132 mm for the slave, respectively. An aluminum bar 25 mm in diameter is fixed to the common base of the master/slave motors for a *rigid* contact at the slave. When soft tissues, *eg.* a human hand, are put between the aluminum bar and the slave, a $flexible$ contact is realized. The control system is implemented at a sampling frequency of 500 Hz on a CPU board in a VME cage running the VxWorks operating system.

Note that the master and the slave are driven by the same motors but with two different gear ratios. In order to make the dynamic properties of Z_m and Z_s close to each other, the position/velocity of the slave is scaled up and the force of the slave is scaled down by a factor of $5(= 50/10)$. Also

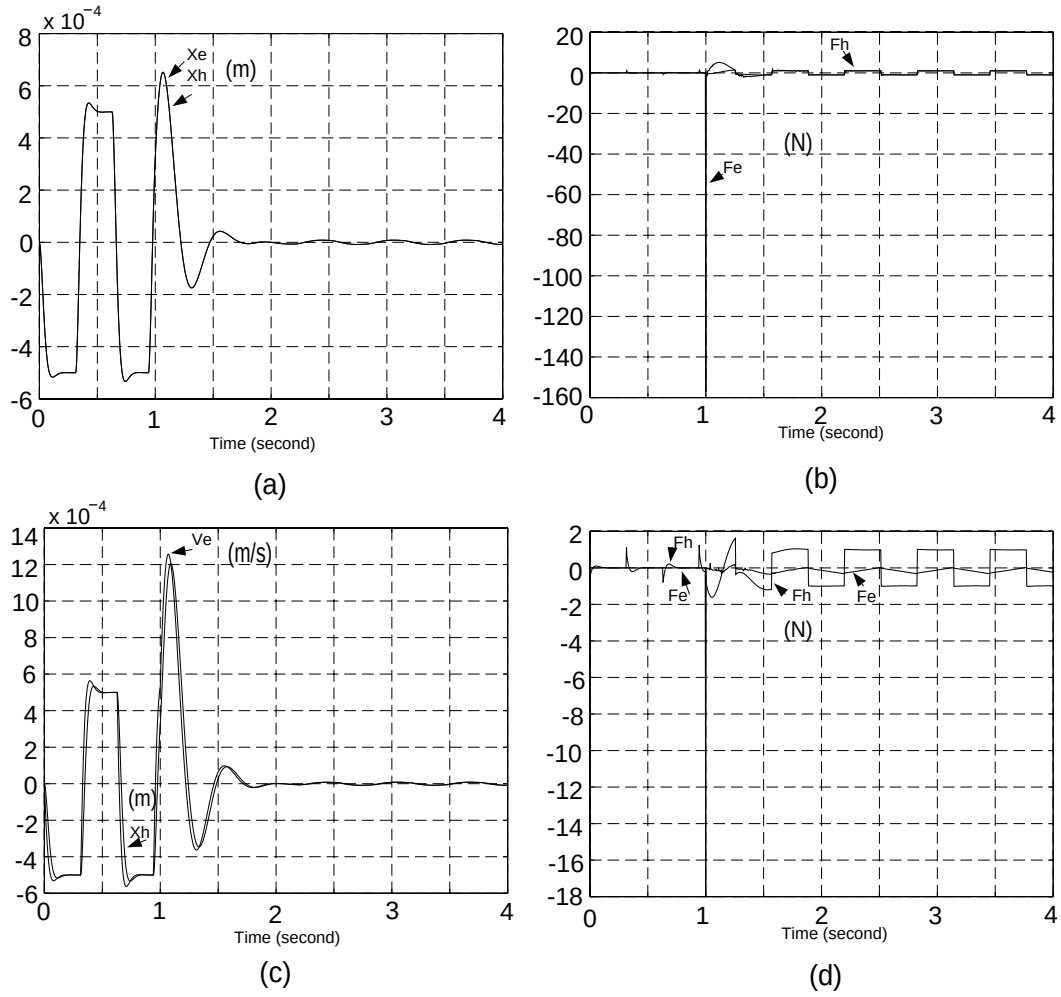

Figure 6: Transparent teleoperation: slave is in free-motion for the first 1 second, and then makes hard contact for the last 3 second. (a) and (b): position control; (c) and (d): rate control.

note that, all the motion/force variables are expressed in motor axes; therefore, position, velocity and force correspond to angular position in radians, angular velocity in radians/second, and torque in Newton-meter, respectively.

7.2 Simulation Results

The master and slave dynamics are modeled as

$$F_{cm} = Z_m V_h + F_{fm} - F_h \tag{37}$$

$$F_{cs} = Z_s V_e + F_{fs} + F_e \ , \tag{38}$$

Figure 7: Photograph of the experimental setup.

where F_{cm} and F_{cs} are the master and slave torques, respectively, and F_{fm} and F_{fs} are friction torque terms. Using an off-line identification method (Tafazoli et al., 1996), the impedances and friction torques in the above were identified as

$$Z_m = 0.0034s \tag{39}$$

$$Z_s = 0.0030s \tag{40}$$

$$F_{fm} = 0.0006V_h + 0.02177sgn(V_h) \tag{41}$$

$$F_{fs} = 0.0359V_e + 0.167sgn(V_e) \ . \tag{42}$$

The hand dynamics model Z_h is the same as the one used in (30), and the environment located at $X_{e0} = 0.4$ radians assumes the impedance model

$$Z_e = 1000 + 10^5/s \tag{43}$$

for a *medium environment* and

$$Z_e = 10^8/s \tag{44}$$

for a *hard environment*. The local position control parameters are chosen as

$$C_m = 0.4 + 4.0/s \tag{45}$$

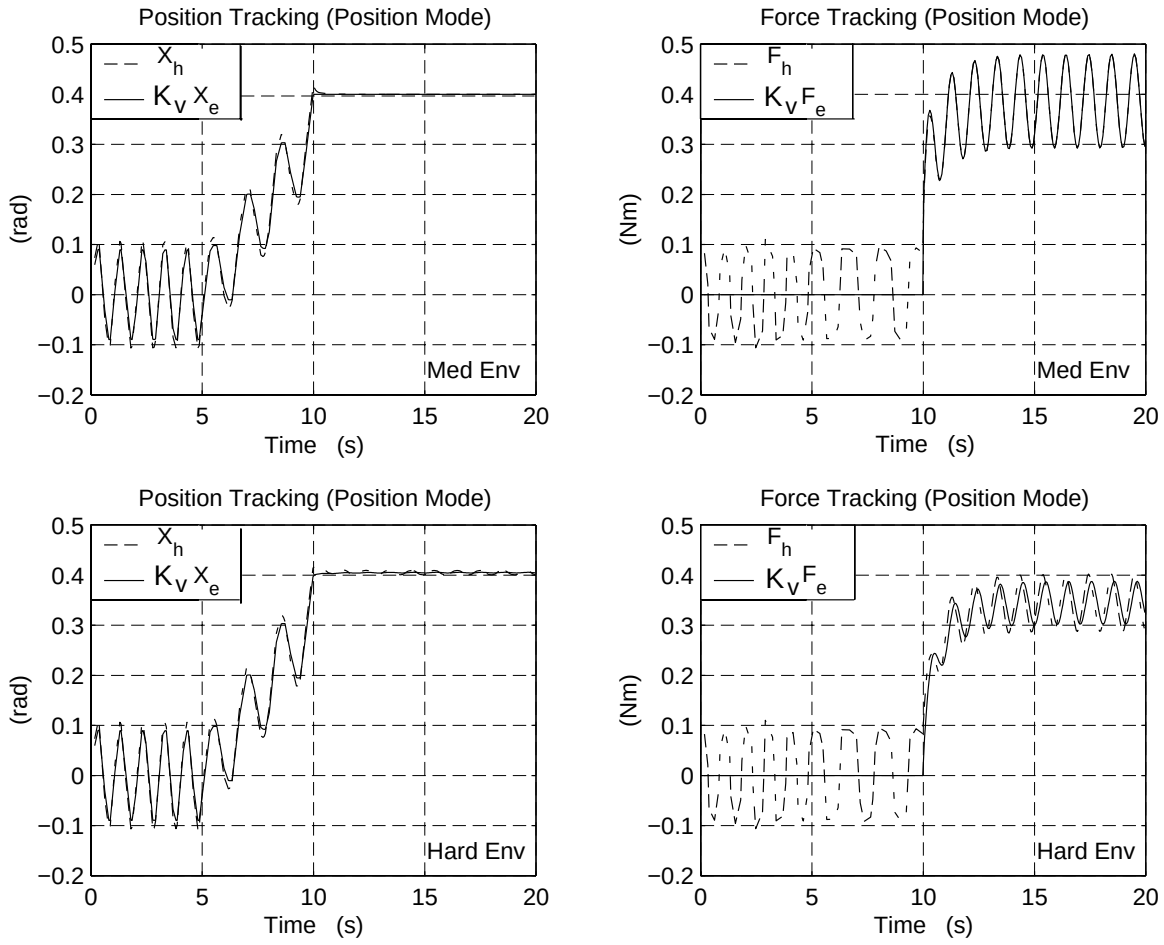

Figure 8: Simulation results of position/force tracking under position control.

$$C_s \quad = \quad 0.5 + 5.0/s \ , \tag{46}$$

while the remote control parameters C_1, C_2, C_3 and C_4 are as in (23), where $G = K_v = 0.2$ for position mode control and $G = 0.2s/(1 + 0.02s)$ for rate mode control.

The simulation results are illustrated in Figure 8 for position control and in Figure 9 for rate control. In Figure 8, the upper/lower two figures correspond to motion from free space to contact with the *medium/hard environment*. The left/right two figures represent position/force master-slave tracking errors for the two different contact environments. As shown in Figure 10-b, the operator exogenous

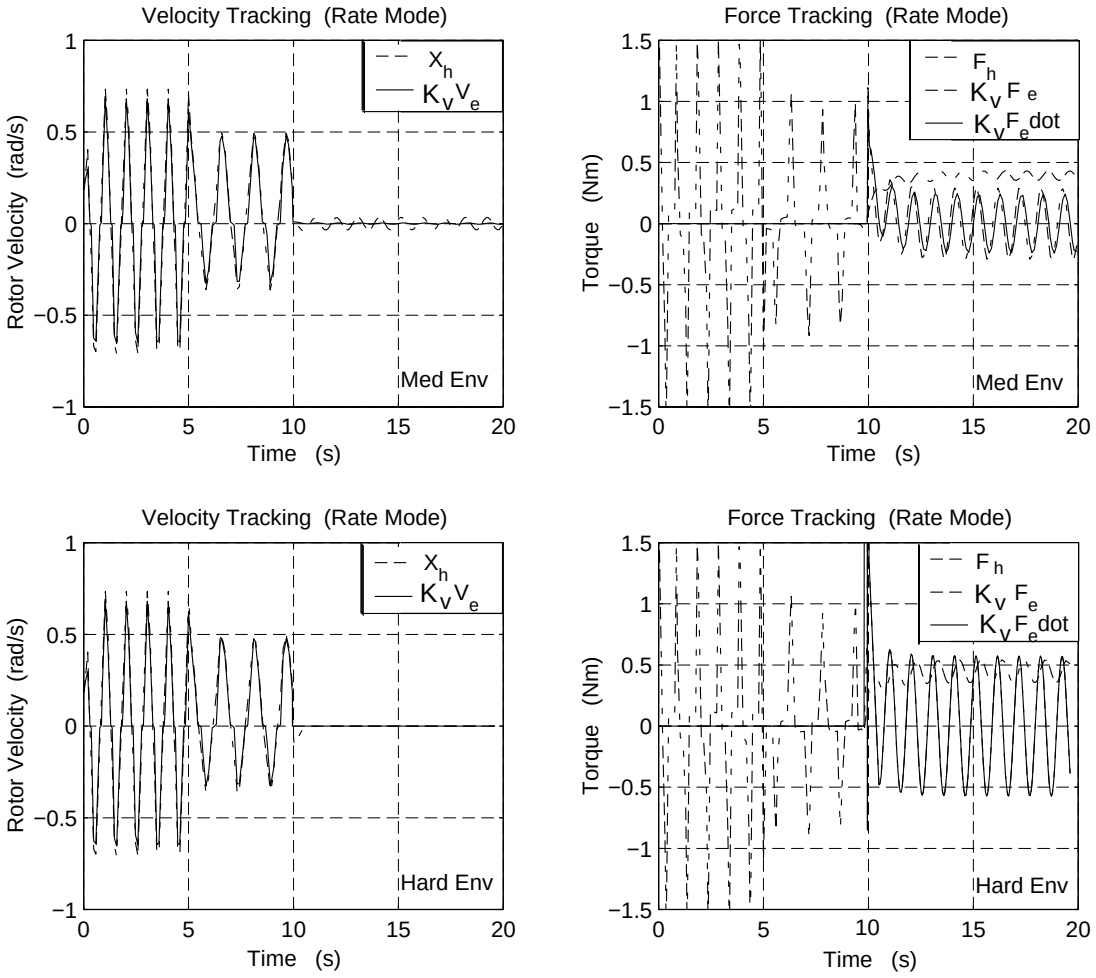

Figure 9: Simulation results of velocity/force tracking under rate control.

force input

$$F_h^* = \begin{cases} 0.1\sin(2\pi t) & 0 < t \leq 5 \\ 0.056(t-5) + 0.089\sin(1.3\pi(t-5)) & 5 < t \leq 10 \\ 0.369 + 0.013(1-e^{(10-t)}) + 0.093\sin(1.95\pi(t-10)) & 10 < t \leq 20 \end{cases} \tag{47}$$

is applied in position control mode to mimic a force profile similar to the one generated from the experiments. Figure 9 illustrates simulation results under rate control where (29) is implemented with $K_v = 0.2$ and $T = 0.02$ and the derivative of (47) is used as F_h^* to make the slave perform a similar task as it did in the position mode simulation. The left/right figures represent velocity/force tracking for the two different contact environments. Note that by using (29), the slave motion is the integral of

the master motion. The simulation results also show very good force tracking performance in contact. In free-motion, good position/velocity tracking can be seen. The significant free-motion force error is mainly due to the uncompensated friction in the gearheads. This will be also noted in the experiments presented in the next sub-section.

7.3 Experimental Results

For position mode control, the same control laws as in (45)-(46) with $G = K_v = 0.2$ have been implemented. The experimental results are illustrated in Figure 10, where the solid lines represent the position/force (X_h and F_h) of the master and the dashed lines represent the scaled position/force ($G\ X_e$ and $G\ F_e$) of the slave. The exogenous input is generated by the operator. Figure 10-a gives the position tracking data, while Figure 10-b presents the force tracking profile. The experiments start from free-motion. At about $t = 4.1$ s, the slave makes contact with a flexible environment (hand palm) and remains in contact until $t = 8.4$ s. Around $t = 10.0$ s, the slave contacts the fixed aluminum bar. The slave positions and forces faithfully track those of the master without loss of stability, even in the case of rigid contact.

The transfer function of the hybrid matrix parameters defined in (25) is plotted in Figure 11 with corresponding coherence functions plotted in Figure 12. Two experiments were conducted to get the hybrid parameters by using force measurements F_h and F_e and position measurements X_h and X_e. The velocities V_h and V_e were obtained by numerical differentiation. In the first experiment the master was controller by the operator, with the slave in free motion. In this case, the slave force F_e is zero. Therefore, based on the force of the master F_h and the encoder readings of two robots, h_{11} and h_{21}, together with their coherence functions, are obtained by using the "spectrum" function in MATLAB. In the second experiment the master was controlled by the operator and the slave was in contact with the aluminium bar. Based on the force and the encoder readings of the master and slave and the previoulsy calculated h_{11} and h_{21} parameters, the remaining hybrid parameters h_{12} and h_{22} and their coherence functions are obtained. In the two experiments, the human operator generated the motions/forces at different frequencies. Each experiment lasted 100 seconds. The data recording rate

was 60 Hz. This yields a frequency resolution of 0.01 Hz and a frequency range of 30 Hz. In Figure 11, $|h_{12}|$ and $|h_{21}|$ are close to 0 db, reflecting excellent transparency for frequencies up to 8 Hz. The parameter h_{11} corresponds to $Z_m \approx 0.003s + 0.05$. The value $0.003s$ is the equivalent mass of the master robot, and is consistent with the identification results of Section 7.2. Similarly, the value 0.05 is the equivalent damping resulting from the motor drive Coulomb and viscous friction. In view of (25), the parameter $h_{22} = (GV_e - V_h)/(GF_e)$ represents the modeling error, likely resulting from backlash and friction. For a small enough motion of the master, the slave linkage does not move. Therefore, with a small but non-zero environment force F_e, the amplitude of the velocity error $GV_e - V_h$ is equal to the amplitude of V_h.

Under rate control, G is given by (29) with $K_v = 0.2$, $T = 0.2$ s. The local control parameters C_m and C_s are the same as in (45) and (46). The experimental results are illustrated in Figure 13. Again the experiments start with free-motion followed by the slave making contact with a flexible environment (hand palm) from $t = 5.3$ s to $t = 9.5$ s, and with the aluminum bar from $t = 11.5$ s onward. In Figure 13-a, the solid line denotes the position of the master, while the dashed line denotes the scaled velocity ($K_v\ V_e$)of the slave. The results show good motion tracking. In Figure 13-b, the solid line represents the master force F_h. The dashed line represents the scaled slave force $K_v\ F_e$. The dash-dot line is the derivative of the dashed line $K_v\dot{F}_e$, which is used to compare with the solid line F_h in order evaluate the force tracking performance.

The hybrid matrix parameters defined by (25) are shown in Figure 14. The experimental procedure described for position control was also followed here. The magnitudes $|h_{12}|$ and $|h_{21}|$ are close to 0 db, reflecting excellent transparency for frequencies up to 8 Hz, whereas h_{11} and h_{22} representing Z_m and the system error are very close to h_{11} and h_{22} in Figure 11. The coherence functions for obtaining Figure 14 are shown in Figure 15, indicating a high degree of confidence for h_{11}, h_{21}, and h_{12} from DC to 8Hz and for h_{22} from 1 Hz to 8 Hz.

7.4 Unilateral Constraint Correction

In rate control, where G is defined by (29), the slave subsystem behaves as an integral of the master subsystem. This causes problems when the slave encounters a stiff or rigid unilateral environment, as the whole teleoperation system exhibits a *sticky* behavior, *i.e.* it is both difficult to move against and away from the environment. In other words, a unilateral constraint at the slave side results in a bilateral constraint at the master side, even though good transparency is achieved according to (19). In order to reflect the unilateral behavior to the master, C_3 in (23) can be modified in the following manner

$$C_3 = \begin{cases} 0 & F_e \cdot X_h < 0 \ \ \& \ \ \mid X_h - K_v \cdot V_e \mid \geq \epsilon \\ \frac{1+Ts}{K_v s} & \text{otherwise} \end{cases} , \tag{48}$$

where ϵ is a small positive constant which gives the threshold for the unilateral constraint correction. The effect of equation (48) is as follows: when a constraint opposes the motion, the controller is unchanged; otherwise, the integral force at the slave side is set to zero to allow the slave to leave the unilateral constraint.

Experimental results implementing (48) are summarized in Figure 16. As expected, when the master is about to leave the unilateral constraint, F_e is instantly nulled out. In the experiments presented here, due to a tight position control and accurate motion tracking of the motors, $|X_e - \int X_h|$ does not grow significantly, even after a long period of pushing the slave against a rigid constraint. If this error does increase, in addition to (48), the slave position command along the constraint can be frozen at contact (Salcudean et al. 1999).

8 Conclusions

The performance of a teleoperator system can be improved significantly by feeding the operator with the slave contact force. With a four-channel data transmission, the task impedance can be faithfully reconstructed at the master side to make the system transparent under ideal conditions. The kinematic correspondence between the master and slave could be more general than just a simple position to

position correspondence. As two special cases in this paper, the design and analysis for achieving transparent teleoperation control system in both position and rate modes are given. In rate control, due to integral action, a unilateral constraint encountered by the slave is displayed as a bilateral contraint at the master. A scheme that nulls out force feedback to the master when the environment force and hand position oppose each other has been shown to fix this problem. Illustrative simulation and experimental results have shown satisfactory position/force and velocity/force tracking under the position and rate modes of operation, respectively. In addition, the spectral analysis of the master-slave two-port network hybrid parameters have been included to demonstrate that the teleoperation system performs as designed.

References

[1] Adams, R. J. and Hannaford, B. 1999. Stable haptic interaction with virtual environments. *IEEE Trans. Rob. & Auto.* 15(3):465-474.

[2] Anderson, R.J. Spong, and M.W. 1989. Bilateral control of teleoperators with time delay. *IEEE Trans. Auto. Contr.* 34:494-501.

[3] Bejczy, A., and Handlykken, M. 1981. Experimental results with a six-degree-of-freedom force-reflecting hand controller. *Proc. 17th Annual Conf. Man. Contr.* Los Angeles, CA.

[4] Daniel, R.W., and McAree, P.R. 1998. Fundamental limits of performance for force reflecting teleoperation. *Int. J. Rob. Res.* 17(8):811-830.

[5] DiMaio, S.P., Salcudean, S.E., Reboulet, C., Tafazoli, S., and Hashtrudi-Zaad, K. 1998. A virtual excavator for controller development and evaluation. *Proc. IEEE Int. Conf. Rob. & Auto. (ICRA'98)* Leuven, Belgium, pp. 52-58.

[6] Fasse, E.D. and Hogan, N. 1994. Quantitative measurements of haptic perception. *Proc. IEEE Int. Conf. Rob. & Auto.* San Diego, CA:IEEE, pp. 3199–3204.

[7] Hannaford, B. 1989. A design framework for teleoperators with kinesthetic feedback. *IEEE Trans. Rob. & Auto.* 5(4):426-434.

[8] Hannaford, B. 1990. Scaling, impedance, and power flows in force reflecting teleoperation. *Rob. Res., ASME DSC* 26:229-232.

[9] Hashtrudi-Zaad, K. and Salcudean, S.E. 2000. Analysis and evaluation of stability and performance robustness for teleoperation control architectures. *Proc. of IEEE Int. Conf. Rob. & Auto. (ICRA'2000).* San Francisco, CA:IEEE, pp.3107-3113.

[10] Hogan, N. 1989. Controlling impedance at the man/machine interface. *Proc. IEEE Int. Conf. Rob. & Auto.* pp. 1626-1631.

[11] Hunter, I.W., Lafontaine, S., Nielsen, P.M.F., Hunter, P.J., and Hollerbach, J.M. 1990. Manipulation and dynamic mechanical testing of microscopic objects using a tele-micro-robot system. *IEEE Contr. Sys. Mag.* 10(2):3-9.

[12] Iwata, H. 1990. Artificial reality with force feedback: development of desktop virtual space with compact master manipulator. *Computer Graphics* 24(4):165-170.

[13] Kazerooni, H. 1990. Human-robot interaction via the transfer of power and information signals. *IEEE Trans. Sys. Man. & Cyber.* 20(2):450-463.

[14] Kazerooni, H., Tsay, T.-I., and Hollerbach, K. 1993. A controller design framework for telerobotic systems. *IEEE Trans. Contr. Sys. Tech.* 1(1):50–62.

[15] Lawrence, D.A. 1993. Stability and transparency in bilateral teleoperation. *IEEE Trans. Rob. & Auto.* 9(5):624-637.

[16] Parker, N.R., Salcudean, S.E. and Lawrence, P.D. 1993. Application of force feedback to heavy duty hydraulic machines. *Proc. IEEE. Int. Conf. Rob. & Auto. (ICRA'93)* Atlanta, GA:IEEE, pp. 375-381.

[17] Salcudean, S.E. and Wong, N.M. 1993. Coarse-fine motion coordination and control of a teleoperation system with magnetically levitated master and wrist. *Experimental Robotics III*, T. Yoshikawa and F. Miyazaki, (Eds.), Spring-Verlag, pp. 28-30.

[18] Salcudean, S.E., Wong, N.M., and Hollis, R. 1995. Design and control of a force-reflecting teleoperation system with magnetically levitated master and wrist. *IEEE Trans. Rob. & Auto.* 11(6):844-858.

[19] Salcudean, S.E., Ku, S., and Bell, G.S. 1997. Performance measurement in scaled teleoperation for microsurgery. *Proc. First Joint Conf. of CVRMED II & MRCAS* Grenoble, France, pp. 789-798.

[20] Salcudean, S.E. 1998. Control for teleoperation and haptic interfaces. in *Control Problems in Rob. & Auto.*, B. Siciliano and K.P. Valavanis (Eds.), Springer-Verlag, LNCIS 230: 51-66.

[21] Salcudean, S.E., Hashtrudi-Zaad, K., Tafazoli, S., DiMaio, S.P., and Reboulet, C. 1999. Bilateral matched-impedance teleoperation with application to excavator control. *IEEE. Contr. Sys. Mag.* 19(6):29-37.

[22] Sirouspour, M. R., DiMaio, S. P., Salcudean, S. E., Abolmaesumi, P., and Jones, C. 2000. Haptic interface control – design issues and experiments with a planar device. *Proc. of IEEE Int. Conf. Rob. & Auto. (ICRA'2000).* San Francisco, CA:IEEE, pp.789-794.

[23] Stokic, D., Vukobratovic, M., and Hristic, D. 1986. Implementation of force feedback in manipulation robots. *Int. J. Rob. Res.* 5:66-76.

[24] Tafazoli, S., De Silva, C.W., and Lawrence, P.D. 1996. Friction modeling and compensation in tracking control of an electrohydraulic manipulator. *Proc. IEEE Mediterranean Symp. New Dir. Contr. & Auto.* Krete, Greece, pp. 375-380,

[25] Yan, J. and Salcudean, S.E. 1996. Teleoperation controller design using H^∞ optimization with application to motion-scaling. *IEEE Trans. Contr. Sys. Tech.* 4(3):244-258.

[26] Yokokohji, Y. and Yoshikawa, T. 1994. Bilateral control of master-slave manipulators for ideal kinesthetic coupling. *IEEE Trans. Rob. & Auto.* 10(5):605-620.

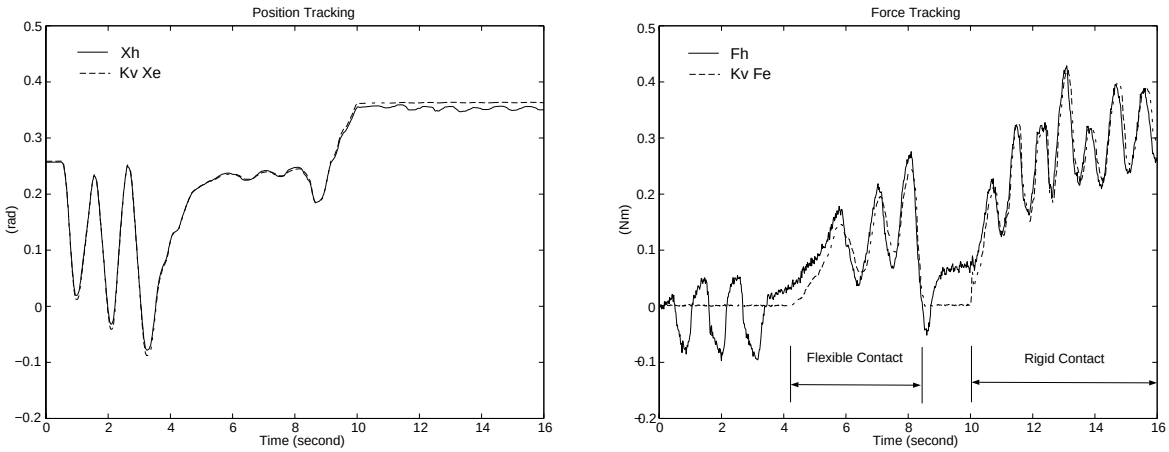

(a) (b)

Figure 10: Experimental results of position/force tracking under position control.

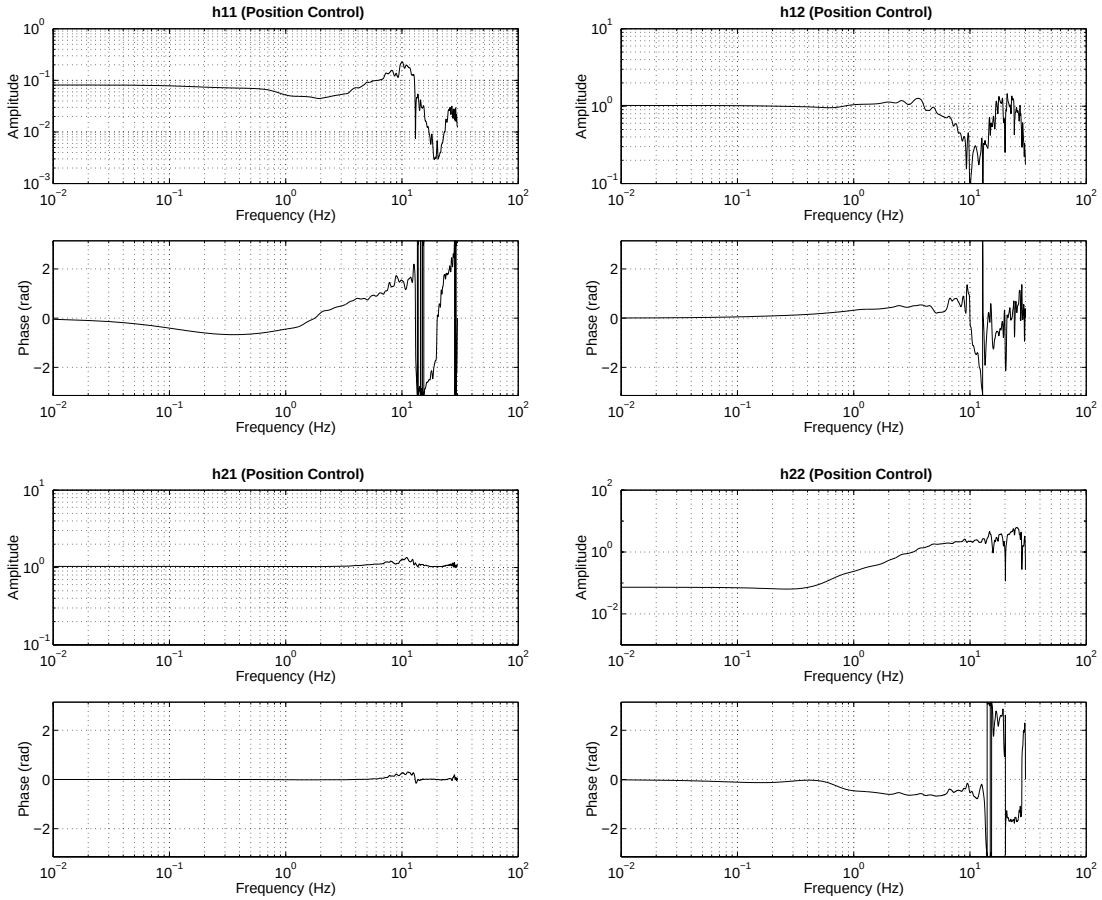

Figure 11: Frequency spectra of the hybrid matrix $H(j\omega)$ under position control.

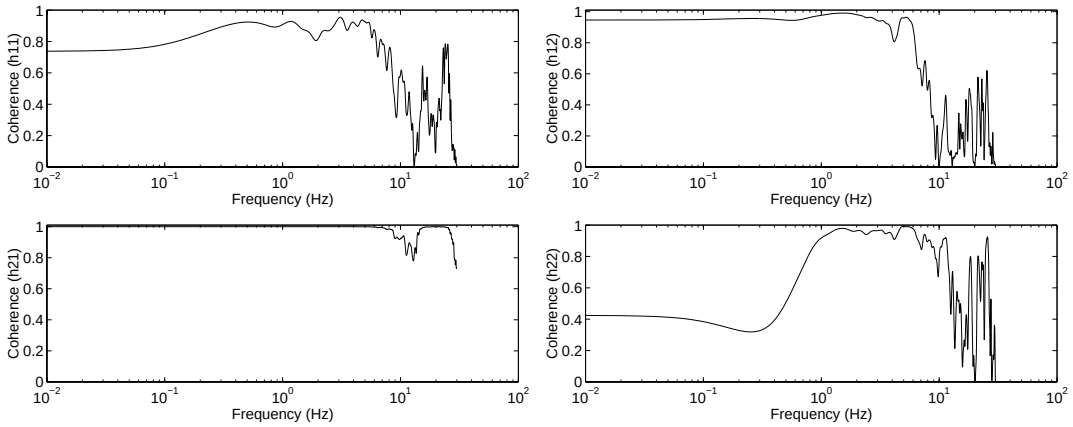

Figure 12: Coherence functions of Figure 11.

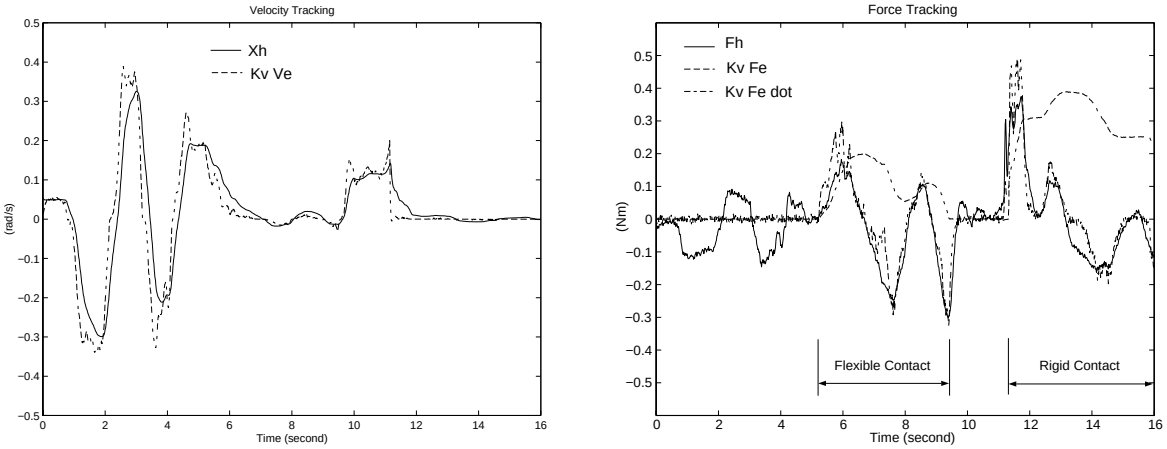

(a) (b)

Figure 13: Experimental results of velocity/force tracking under rate control.

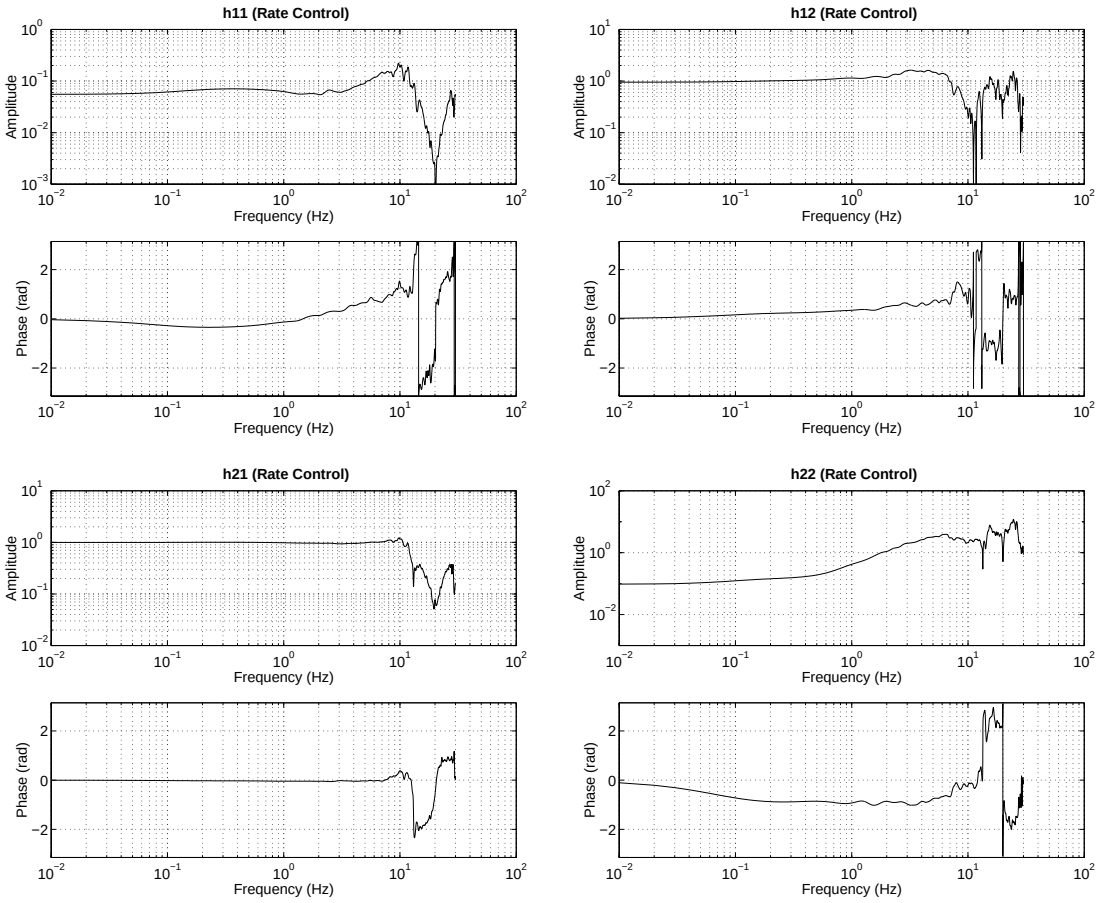

Figure 14: Frequency spectra of the hybrid matrix $H(j\omega)$ under rate control.

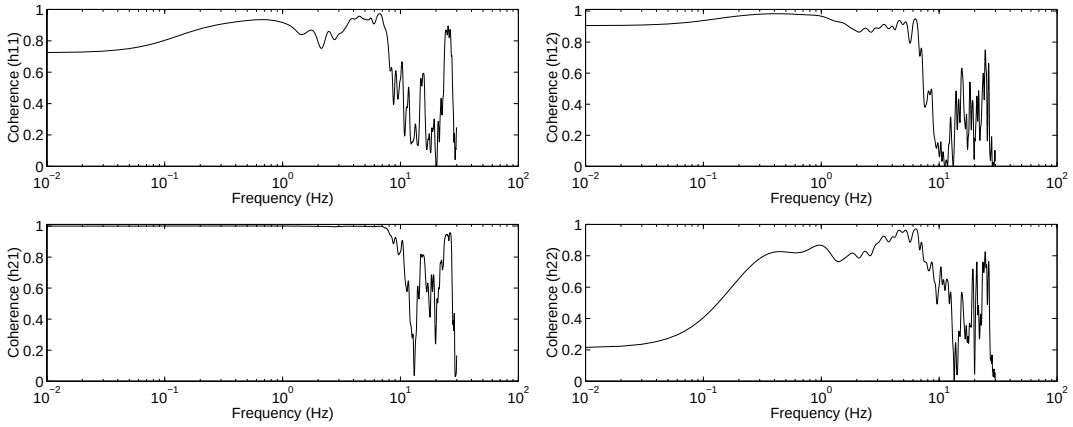

Figure 15: Coherence functions of Figure 14

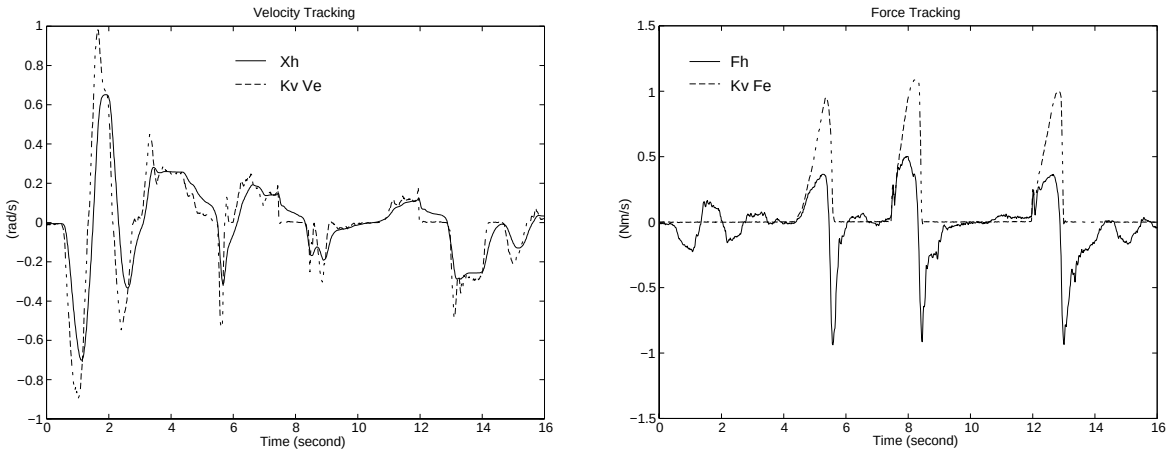

(a) (b)

Figure 16: Experimental results of velocity/force tracking under rate control with unilateral correction.